Progress In Electromagnetics Research M, Vol. 55, 1–12, 2017

Transitional Behaviors of CQGLE Solitons across Boundaries on a Phase Plane

Huai-Ming Chang and Jean-Fu Kiang*

Abstract—Soliton solutions of a cubic-quintic Ginzburg-Landau equation (CQGLE) are computed and analyzed on a parametric plane, specifically across the transitional zones that separate regions associated with different types of solitons. The transformations of behaviors in these transitional zones between stationary and pulsating regions are characterized by the total pulse energy and its maximum value. It is also found that the initial pulse waveform has little effect on bifurcation and the valid range of initial amplitude.

1. INTRODUCTION

The solitons present in a mode-locked laser can be categorized into conventional and dissipative types [1]. The conventional solitons are formed via the balance of nonlinearity (mainly third-order) and dispersion mechanisms. On the other hand, dissipative solitons involve more factors, including dispersion, gain/loss and nonlinearities of different orders. The conventional solitons can be represented in terms of a set of eigen-solutions, while the dissipative solitons appear to be independent of each other and prone to instability, sometimes leading to chaos or disappearance.

Various types of dissipative solitons were found, including stationary, pulsating and chaotic types [2–4]. A cubic-quintic (CQGLE) or its variation was used to model dissipative solitons in passively mode-locked lasers [5–9]. An exploding soliton is an extreme example of pulsating solitons, which is usually quasi-stable and will grow rapidly over some period [10, 11]. In [10], exploding solitons and their spectrum were measured in a laser cavity.

Various soliton types were presented on a parametric plane [12]. For example, a bifurcation diagram was presented to show periodic non-chaotic explosions and period-halving process [11]. A total energy Q was defined to characterize the behaviors of these solitons. Boundaries between soliton types on a parametric plane were observed [12], and the transitional behaviors across these boundaries were reported, for example, the bifurcation across the boundary between a pulsating region and a chaotic region. More details on the transitional behaviors across these boundaries will provide useful information for better understanding these solitons.

Bifurcation phenomena have been observed and discussed [13–15]. In [13], an experiment was set up to verify the prediction with the CQGLE. As the controlling parameters are changed continuously on a parametric plane, the solution may transit from pulsating to period-doubling, period-quadrupling, and eventually to chaotic type. In [15], different parametric planes were used to categorize solitons obtained by solving the CQGLE, and boundaries dividing different types of solitons were drawn [14].

A creeping soliton with non-zero drift velocity [16] evolves from a pulsating soliton with zero drift velocity. Sometimes, the center of soliton drifts back and forth in time as the soliton evolves along its propagating path. A creeping soliton can bifurcate into two or more branches before turning chaotic.

Received 22 November 2016, Accepted 8 February 2017, Scheduled 22 February 2017
* Corresponding author: Jean-Fu Kiang (jfkiang@ntu.edu.tw).
The authors are with the Graduate Institute of Communication Engineering, National Taiwan University, Taipei, Taiwan, R.O.C..

It can also break into a pulsating soliton with zero drift velocity and another creeping soliton with non-zero drift velocity.

In this work, different types of dissipative solitons obtained by solving the CQGLE are studied. The behaviors in the transitional zones across a boundary between two adjacent regions on a typical parametric plane are investigated. This work is organized as follows. A brief review of the CQGLE and the simulation setup are presented in Section 2, the transition between pulsating and no-solution regions is presented in Section 3, the transition between stationary and pulsating regions is presented in Section 4, and the effects of initial waveform and amplitude are presented in Section 5. Finally, some conclusions are drawn in Section 6.

2. BRIEF REVIEW OF THEORETICAL MODEL AND SIMULATION SETUP

A cubic-quintic complex Ginzburg-Landau equation (CQGLE) was proposed to describe the normalized electric field ψ in a passively mode-locked laser as [12]

$$\frac{\partial\psi}{\partial z} = -j\frac{D}{2}\frac{\partial^2\psi}{\partial t^2} - j|\psi|^2\psi - j\nu|\psi|^4\psi + \delta\psi + \xi|\psi|^2\psi + \tau\frac{\partial^2\psi}{\partial t^2} + \mu|\psi|^4\psi \tag{1}$$

where t is the normalized delay time in the frame moving with the group velocity; z is the normalized propagation distance along the laser cavity; D denotes the cavity dispersion, with $D > 0$ for anomalous dispersion and $D < 0$ for normal dispersion; ν is the quintic nonlinear coefficient; δ denotes linear gain if $\delta > 0$ and loss if $\delta < 0$; τ is the gain-bandwidth coefficient; ξ and μ are the gain coefficients, of cubic and quintic orders, respectively.

The normalized variables ψ, z and t in Eq. (1) are related to their actual counterparts $\tilde{\psi}$, $\tilde{z}$ and $\tilde{t}$, respectively, as

$$\psi = \frac{\tilde{\psi}}{\sqrt{P_0}}, \quad z = \frac{\tilde{z}}{L_d}, \quad t = \frac{\tilde{t}}{t_0}$$

where the time scale t_0 is the full-width half-magnitude (FWHM) pulse width; $L_d = t_0^2/|\beta_2|$ is the length scale of dispersion, which is the distance that a pulse of width t_0 is broadened by a factor of $\sqrt{2}$ due to dispersion β_2, in the absence of nonlinearity; β_2 is the second-order dispersion coefficient; $P_0 = 1/(\gamma L_d)$ is a power scale, which induces a nonlinear phase shift of 1 radian to a pulse propagating over a distance L_d under nonlinear effects; γ is the third-order nonlinear coefficient or the Kerr coefficient. Hence, the parameters D, ν, τ, δ, ξ and μ are related to the parameters β_2, γ, γ_1, g_0, g_1, g_2 and ℓ as [17]

$$\begin{aligned} D &= \frac{\beta_2 L_d}{t_0^2}, \quad \nu = -\gamma_1 P_0, \quad \tau = \frac{g_0 L_d}{\Omega_g^2 t_0^2} \\ \delta &= g_0 L_d, \quad \xi = -\frac{g_1}{\gamma}, \quad \mu = \frac{g_2 P_0}{\gamma} \end{aligned} \tag{2}$$

where g_0 is the linear gain/loss; g_1 is the nonlinear gain/loss; g_2 is the nonlinear gain/loss saturation; γ_1 is the saturation of γ; Ω_g is a bandwidth filtering coefficient.

The actual gain g is inversely proportional to the input power P as $g = g_0/(1 + P/P_{\text{sat}})$, with P_{sat} the saturation power [17], which can be approximated as

$$g \simeq g_0\left[1 - \frac{P}{P_{\text{sat}}} + \left(\frac{P}{P_{\text{sat}}}\right)^2\right] = g_0 - g_1|\tilde{\psi}|^2 + g_2|\tilde{\psi}|^4 \tag{3}$$

where $g_1 = g_0/P_{\text{sat}}$ and $g_2 = g_0/P_{\text{sat}}^2$. The CQGLE is an extension of the nonlinear Schrödinger equation (NLSE), with the linear gain g_0 augmented with higher-order terms, g_1 and g_2. In this work, the symbols g_0, g_1 and g_2 are normalized to become δ, ξ and μ, respectively, as shown in Eq. (2).

A split-step Fourier method (SSFM) is applied to solve Eq. (1) numerically, in which the nonlinear terms and the linear terms are implemented in the time domain and the frequency domain, respectively [18]. The step intervals Δz and Δt are sufficiently small to ensure convergent results.

3. TRANSITION BETWEEN PULSATING AND NO-SOLUTION REGIONS

Figure 1(a) shows a map of soliton types on a μ-D plane [12], where a pulsating/no-solution boundary and a stationary/pulsating boundary are marked. The input waveform is chosen as $\psi(0,t) = 2\,\mathrm{sech}(t/t_0)$, with $t_0 = 0.3$. Fig. 1(b) shows an enlarged map around point 2, where the soliton type varies drastically. We will first investigate the behaviors of solitons near boundary 1 in this Section. Boundary 1 is composed of several transition zones, labeled as pulsating, two-branch bifurcation, four-branch bifurcation and chaotic zones, progressively, as the absolute value of nonlinear gain saturation ($|\mu|$) is decreased from 0.001050 to 0.001002.

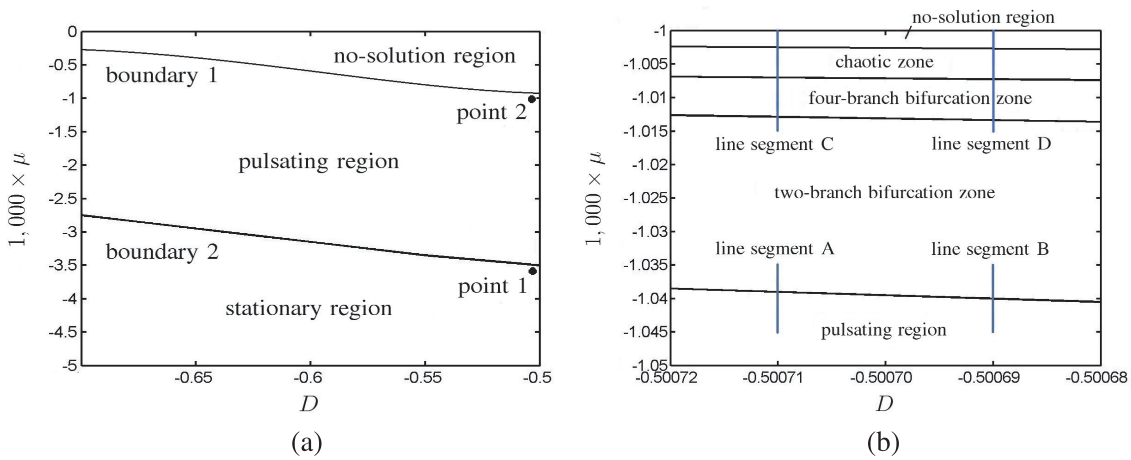

Figure 1. (a) A map of soliton type in the μ-D plane [12], where boundary 1 divides pulsating and no-solution regions, and boundary 2 divides stationary and pulsating regions, (b) enlarged map around point 2, $\psi(0,t) = 2\,\mathrm{sech}(t/t_0)$ with $t_0 = 0.3$, $(\nu, \delta, \xi, \tau) = (0.1, -0.1, 0.95, 0.125)$.

Define the total energy of a soliton as

$$Q(z) = \int_{-\infty}^{\infty} |\psi(z,t)|^2 dt \tag{4}$$

and local maxima and local minima of Q are denoted as Q_M and Q_m, respectively. Fig. 2 shows the spatial evolution of Q. Fig. 2(a) shows that the spatial variation of total energy follows a pattern after the soliton propagates over certain distance. As shown in Fig. 2(b), the value of Q_M reaches 104.45 or 104.4 alternatively, displaying a two-branch bifurcation. The value of Q_m also displays two-branch bifurcation, as shown in Fig. 2(c). The change of Q_M is about 0.05 between alternations, while that of Q_m is only 0.0005, about two orders of magnitude smaller than that in Q_M.

Figure 3 shows the value of Q_M versus μ along line segment A marked in Fig. 1(b). A two-branch bifurcation appears at $\mu = -0.001039$, where Q_M alternates between two values. The soliton takes a longer propagation distance to settle near this point than at other μ's. The value of Q_M versus μ along line segment B marked in Fig. 1(b) is also shown. A two-branch bifurcation appears at $\mu = -0.001040$, slightly smaller than that along line segment A, which implies that the boundary shown in Fig. 1(b) is tilted. The bifurcation with $D = -0.50069$ (dashed curve) appears at larger $|\mu|$ than that with $D = -0.50071$ (solid curve). Also, the Q_M value before the two-branch bifurcation with $D = -0.50069$ is slightly larger than that with $D = -0.50071$. A smaller second-order dispersion ($|D|$) leads to stronger nonlinear gain, thus a higher Q_M and a wider separation after bifurcation in $-0.001039 \leq \mu \leq -0.001035$.

As the value of μ is changed from -0.001035 to -0.001015, the two branches in Fig. 3 are separated farther apart, and four-branch bifurcation appears around $\mu = -0.001015$, as shown in Fig. 4. The range $-0.001015 \leq \mu \leq -0.001010$ is represented by the lower line segments C and D in Fig. 1(b). Before the upper and the lower branches split, their associated Q_M are about 107.25 and 101.2, respectively.

Similar to Fig. 3, the difference of Q_M values in the two branches after bifurcation with $D = -0.50069$ is larger than that with $D = -0.50071$. The bifurcation occurs at $\mu = -0.001013$ with

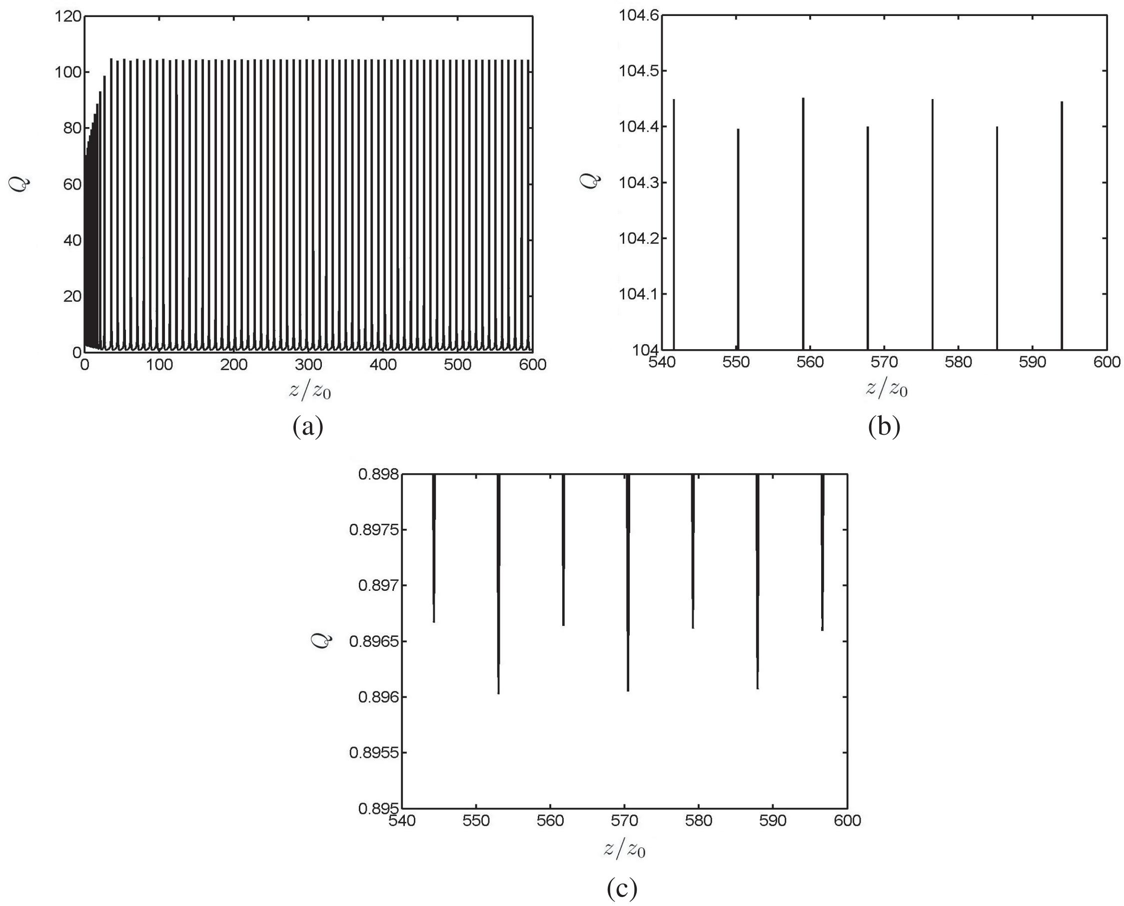

Figure 2. (a) Spatial evolution of Q in $0 \leq z/z_0 \leq 600$, (b) enlarged plot around Q_M in $540 \leq z/z_0 \leq 600$ and (c) enlarged plot around Q_m in $540 \leq z/z_0 \leq 600$; $\mu = -0.001038$, $D = -0.50071$, other parameters are the same as in Fig. 1.

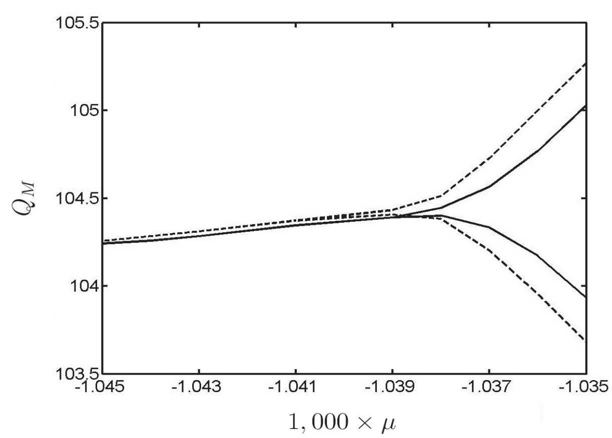

Figure 3. Q_M versus μ along line segment A in Fig. 1(b), $D = -0.50071$ (———) and along line segment B in Fig. 1(b), $D = -0.50069$ (– – –); other parameters are the same as in Fig. 1.

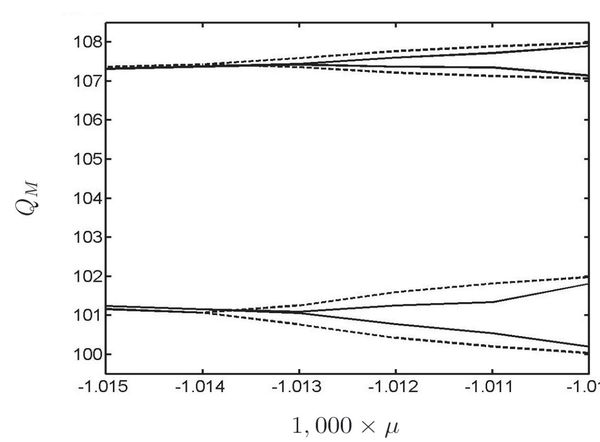

Figure 4. Q_M versus μ along lower line segment C in Fig. 1(b), ———: $D = -0.50071$, – – –: $D = -0.50069$; other parameters are the same as in Fig. 1.

$D = -0.50071$, and occurs at $\mu = -0.001014$ with $D = -0.50069$. The boundary between the two-branch and the four-branch zones is also tilted, as shown in Fig. 1(b).

Figure 5(a) shows the values of Q_M versus μ along the upper line segment C in Fig. 1(b), with $D = -0.50071$. The four branches split into eight branches at $\mu = -0.001008$. At $\mu \simeq -0.00100675$, bifurcation into ten branches occurs. At $\mu \simeq -0.0010065$, the bifurcation turns to chaotic (non-periodic). At $\mu \simeq -0.00100625$, a twelve-branch bifurcation emerges from chaotic.

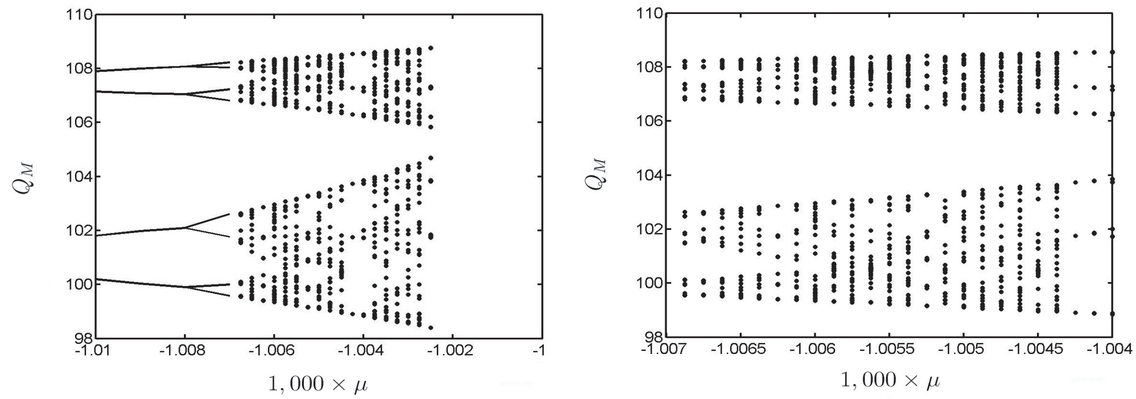

Figure 5. (a) Q_M versus μ along upper line segment C in Fig. 1(b), (b) enlarged plot with $-1.007 \leq 1,000 \times \mu \leq -1.004$; $D = -0.50071$, other parameters are the same as in Fig. 1.

Both the ten-branch and twelve-branch states appear within a very narrow interval of μ. Fig. 5(b) shows an enlarged plot, where splitting and merging of branches occur over a small interval of μ, which is typical in a chaotic zone. At $\mu = -0.00100425$, an indefinite number of branches in a chaotic zone suddenly merge to six branches. At $\mu = -0.0010025$, all eight branches suddenly vanish, beyond which is the no-solution region where an initial waveform will vanish after propagating over a sufficiently long distance.

Figure 6 shows the spatial evolution of Q in the no-solution region. The soliton propagates to about $z/z_0 = 30$ and monotonically decreases to zero. The boundary between the no-solution region and the chaotic zone with $D = -0.50071$ and $D = -0.50069$ are $\mu = -0.0010024$ and $\mu = -0.001027$, respectively. As a soliton enters the chaotic zone, $|\mu|$ is too small to sustain a pulsating soliton. When $|\mu|$ is further decreased, the nonlinear gain ξ will dominate μ, breaking the gain-loss balance and suppressing the soliton.

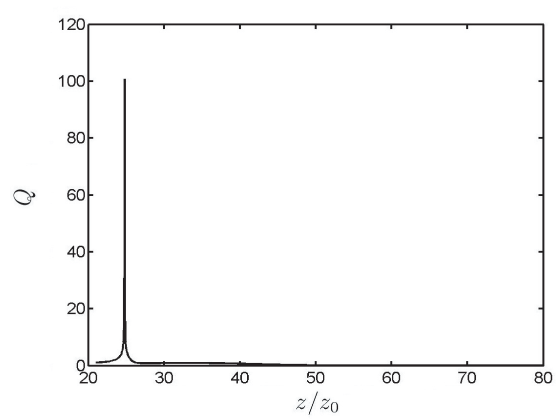

Figure 6. Spatial evolution of Q in the no-solution region; $(D, \nu, \delta, \xi, \mu, \tau) = (-0.5007, 0.1, -0.1, 0.95, -0.001, 0.125)$, initial waveform is $\psi(0, t) = 2\,\text{sech}(t/t_0)$.

4. TRANSITION BETWEEN STATIONARY AND PULSATING REGIONS

Next, consider the boundary between the pulsating and the stationary regions. Fig. 7 shows the evolution of solitons with μ varied around point 1 marked in Fig. 1(a). Fig. 7(a) shows a pulsating soliton with

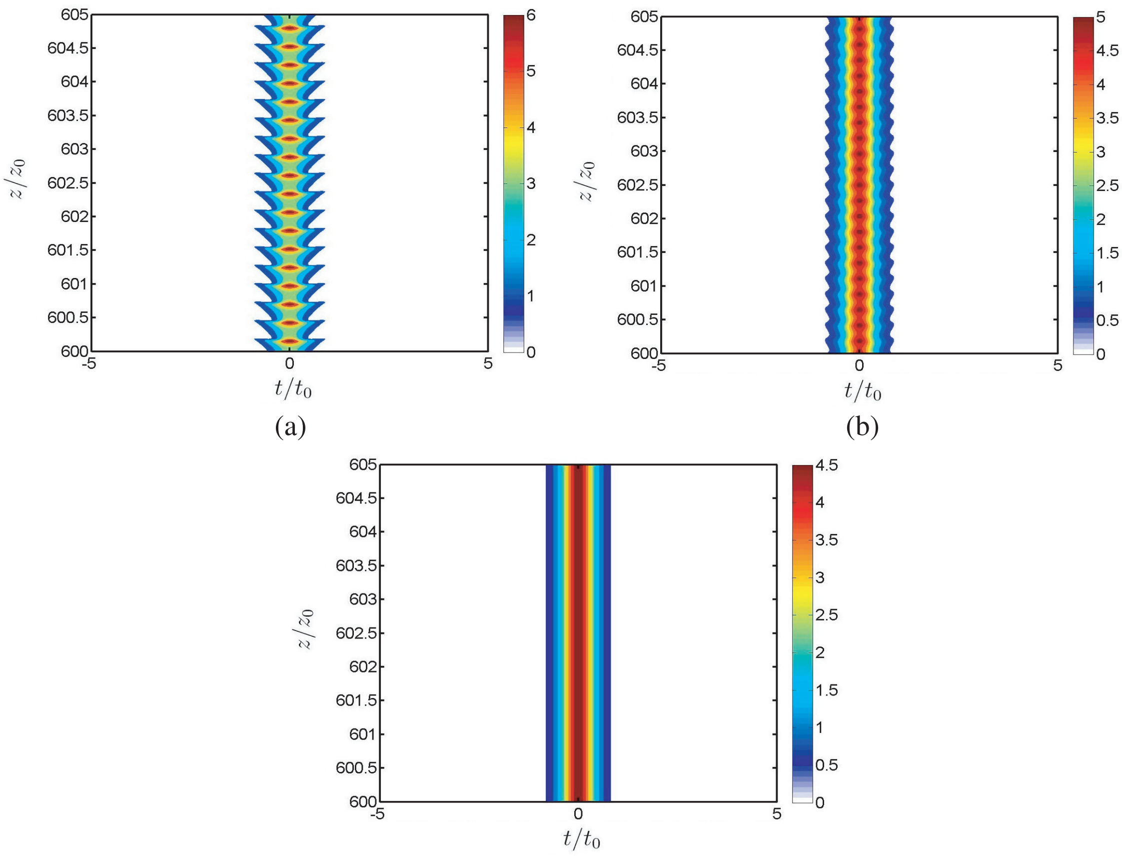

Figure 7. Evolution of soliton at (a) $\mu = -0.003$, (b) $\mu = -0.0035$ and (c) $\mu = -0.004$; $(D, \nu, \delta, \xi, \tau) = (-0.5007, 0.1, -0.1, 0.95, 0.125)$.

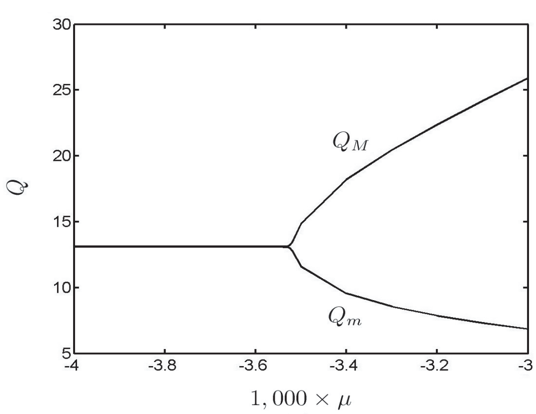

Figure 8. Q versus μ with $-0.004 \leq \mu \leq -0.003$ and $D = -0.5007$, other parameters are the same as in Fig. 1.

$\mu = -0.003$, Fig. 7(c) shows a stationary soliton with $\mu = -0.004$, and Fig. 7(b) shows a soliton with $\mu = -0.0035$, which indicates a gradual progress between those in Figs. 7(a) and 7(c). The pulsating behavior is obvious with $\mu = -0.003$, and becomes moderate as μ changes towards $\mu = -0.004$. It is also observed that with $\mu = -0.003$, the amplitude at the pulse center ($t = 0$) undulates with z/z_0 at large swing. On the other hand, the amplitude at the pulse center with $\mu = -0.004$ remains constant.

Figure 8 shows the Q values with $D = -0.5007$ and μ is changed from -0.004 to -0.003, marked in Fig. 1(a). At $\mu \simeq -0.003525$, the soliton begins to transform from a stationary type (with single Q value) to a pulsating type (with Q value varying periodically between Q_M and Q_m). The difference between Q_M and Q_m increases as the magnitude of nonlinear gain saturation, $|\mu|$, decreases. A wider separation between Q_M and Q_m indicates pulsation with a larger swing. Similar to the bifurcation phenomenon discussed in the last section, it takes a longer propagation distance for a soliton to settle when μ is closer to the bifurcation point.

5. EFFECTS OF INITIAL WAVEFORM AND AMPLITUDE

In this section, we will study the effects of the initial waveform at $z = 0$ and its amplitude on the spatial evolution of solitons. For continuous-wave solutions of CQGLE, there exist a lower bound and an upper bound of amplitude [19]. The initial waveform chosen to compute the results shown in Fig. 6 is $\psi(0, t) = 2\,\mathrm{sech}(t/t_0)$, which vanishes after propagating over certain distance. Fig. 9 shows the solution with the same initial waveform, but its amplitude is doubled, as $\psi(0, t) = 4\,\mathrm{sech}(t/t_0)$. It is observed that the amplitude gradually increases along z and turns into a pulsating-like soliton. It is also found that a lower amplitude fails to sustain a soliton. But will there be an upper bound of amplitude that prevents a soliton from emerging?

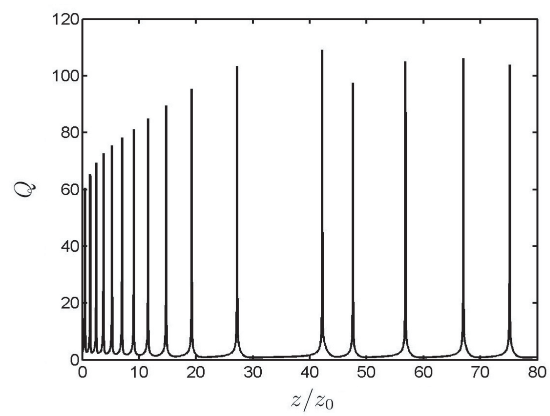

Figure 9. Q-z plot with initial waveform $\psi(0, t) = 4\,\mathrm{sech}(t/t_0)$; $(D, \nu, \delta, \xi, \mu, \tau) = (-0.5007, 0.1, -0.1, 0.95, -0.001, 0.125)$.

Figure 10 shows the distribution of Q_M with an initial waveform $\psi(0, t) = A\,\mathrm{sech}(t/t_0)$ at five different initial amplitudes within $2 \leq A \leq 5$. A chaotic solution is found within the range of $2.7 \leq A \leq 4.2$, and no soliton can be sustained if A falls outside of this range.

To better understand the effects of initial amplitude on sustaining solitons, consider a few points along a line segment in Fig. 1(a), with $D = -0.6$ and $-0.004 \leq \mu \leq -0.001$. Fig. 11 shows the allowable values of Q_M versus A, with $\mu = -0.001$. It is found that a pulsating soliton with $Q_M = 97.52$ appears over $1.3 \leq A \leq 11.9$, $13.6 \leq A \leq 16.5$, $18.9 \leq A \leq 20.9$ and $23.9 \leq A \leq 25.1$. Similarly, at $\mu = -0.002$, $Q_M = 53.51$ over $1.2 \leq A \leq 12.9$, $14.8 \leq A \leq 18.3$ and $21.0 \leq A \leq 23.7$. At $\mu = -0.003$, $Q_M = 23.91$ over $1.2 \leq A \leq 14$, $15.8 \leq A \leq 20.4$ and $23.1 \leq A \leq 27.2$. Note that the value of Q_M is independent of A in all the above cases with different μ's. At $\mu = -0.004$, a stationary soliton appears with $Q = 16.85$ over $1.2 \leq A \leq 15.2$, $16.7 \leq A \leq 22.7$ and $25.4 \leq A \leq 31.4$. The results with different μ's reveal the same characteristics as those shown in Fig. 11, except the valid subranges of A and the values of Q_M are different.

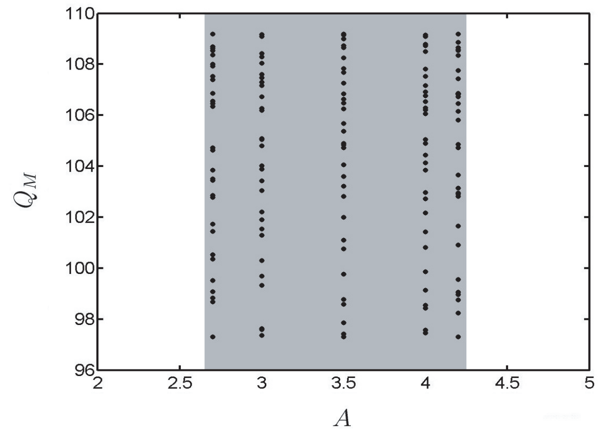

Figure 10. Distribution of Q_M with initial waveform $\psi(0, t) = A\,\text{sech}(t/t_0)$ at five different initial amplitudes; $(D, \nu, \delta, \xi, \mu, \tau) = (-0.5007, 0.1, -0.1, 0.95, -0.001, 0.125)$.

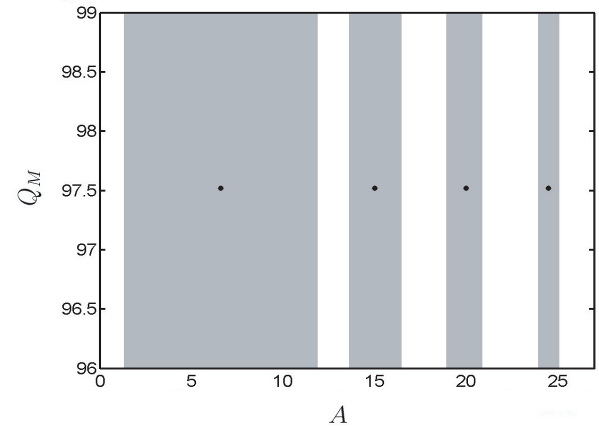

Figure 11. Q_M versus A with $(D, \nu, \delta, \xi, \mu, \tau) = (-0.6, 0.1, -0.1, 0.95, -0.001, 0.125)$. The shaded areas indicate where solitons are allowed, and the dots mark the allowable Q_M values within the shaded areas.

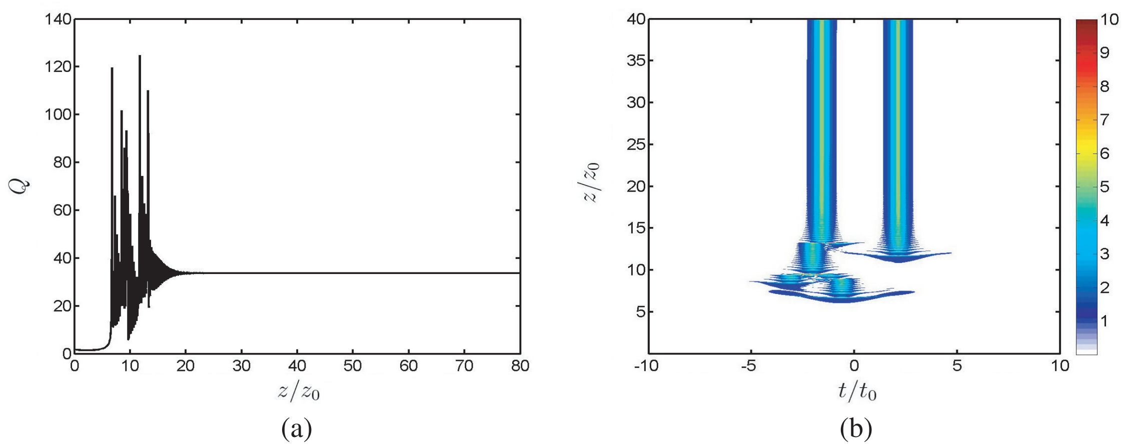

Figure 12. (a) Q versus z and (b) evolution of ψ, $A = 22.7$, $(D, \nu, \delta, \xi, \mu, \tau) = (-0.6, 0.1, -0.1, 0.95, -0.004, 0.125)$.

Figure 12 shows an interesting case with $\mu = -0.004$ and $A = 22.7$. It is observed that the Q value changes dramatically over the interval $6 \leq z/z_0 \leq 15$, and then converges to 33.71 at $z/z_0 > 20$, which is twice the Q value with $A < 22.7$. By taking a closer look at Fig. 12(b), two identical solitons emerge at $z/z_0 > 15$, which explains why the Q value is doubled. Similar phenomenon is also observed near the upper bound of the higher subrange, $A = 31.3$. This sudden emergence of soliton indicates the system is very unstable with this set of parameters, including the initial waveform and its amplitude.

Next, we will investigate the effects of initial amplitude on the soliton behavior as μ varies along line segment C in Fig. 1(b), with $D = -0.50071$ and $-0.00105 \leq \mu \leq -0.001$. The following values of μ are chosen, $\mu = -0.001040$ near the two-branch bifurcation point, $\mu = -0.001020$ inside the two-branch bifurcation zone and $\mu = -0.001010$ inside the four-branch bifurcation zone.

Figure 13 shows the distributions of Q_M at these three μ values, with $2 \leq A \leq 5$. When A is increased to its upper bound, $A = 25.4$, the values of Q_M remain the same. The simulated results are $Q_M \simeq 104.37$ (the value slightly varies since the bifurcation is about to appear) at $\mu = -0.001040$, $Q_M = 101.68, 106.98$ (two-branch zone) at $\mu = -0.001020$, and $Q_M = 100.19, 107.14, 101.80, 107.89$ (four-branch zone) at $\mu = -0.001010$. The values of Q_M remain the same over the range $1.2 \leq A \leq 25.5$

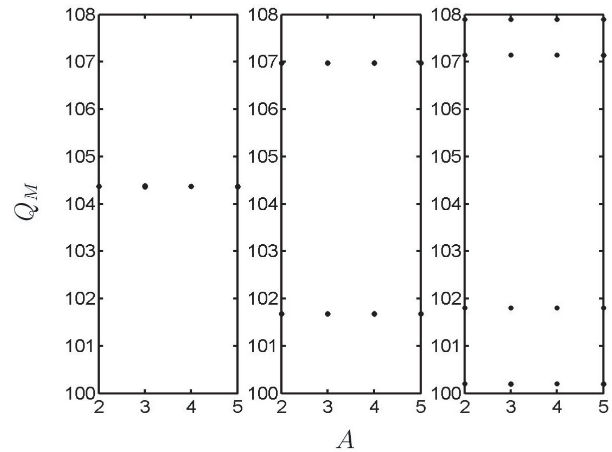

Figure 13. Distributions of Q_M with $2 \leq A \leq 5$, other parameters are the same as in Fig. 3. The values of μ, from the left figure to the right, are $\mu = -0.001040$, $\mu = -0.001020$ and $\mu = -0.001010$, respectively.

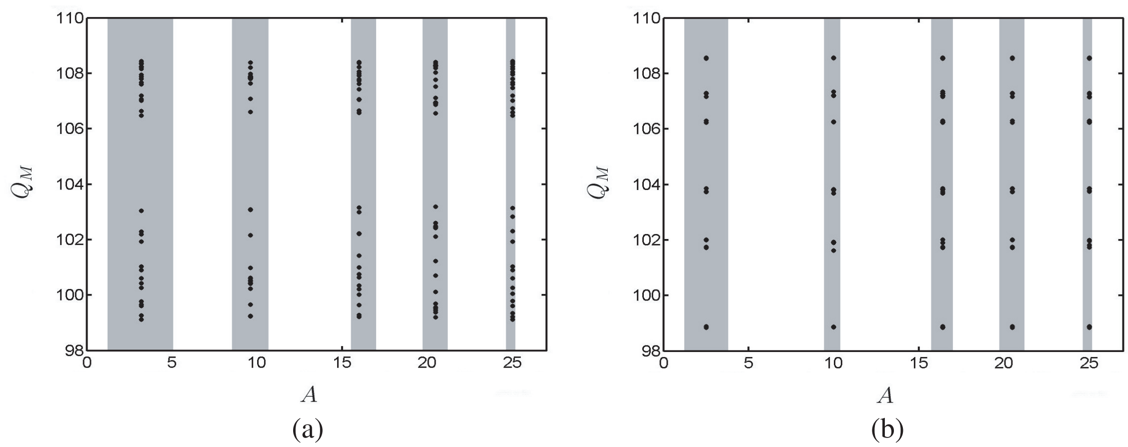

Figure 14. Q_M versus A with (a) $\mu = -0.001005$ and (b) $\mu = -0.001004$; $(D, \nu, \delta, \xi, \tau) = (-0.50071, 0.1, -0.1, 0.95, 0.125)$. The shaded areas indicate where solitons are allowed and the dots mark the allowable Q values, which are the same in the shaded areas.

at $\mu = -0.001040$ and $\mu = -0.001020$, and over the range $1.2 \leq A \leq 25.4$ at $\mu = -0.001010$. Note that solitons exist only over certain subranges of A.

Figure 14 shows the values of Q_M versus A in a chaotic zone with $\mu = -0.001005$ and $\mu = -0.001004$, respectively. At $\mu = -0.001005$, the allowable range of A is consisted of five separate subranges, $1.2 \leq A \leq 5.1$, $8.5 \leq A \leq 10.7$, $15.5 \leq A \leq 17$, $19.7 \leq A \leq 21.2$ and $24.6 \leq A \leq 25.2$. The values of Q_M in these five subranges are clustered within $99.1 \leq Q_M \leq 103.4$ and $106.5 \leq Q_M \leq 108.4$. Similarly, at $\mu = -0.001004$, the allowable range of A is also consisted of five subranges, $1.2 \leq A \leq 3.8$, $9.4 \leq A \leq 10.4$, $15.7 \leq A \leq 17$, $19.7 \leq A \leq 21.2$ and $24.6 \leq A \leq 25.2$. The values of Q_M in these five subranges are clustered around $98.9, 102.0, 103.9, 106.2, 107.2$ and 108.5. As far as these two different μ's are concerned, the type of soliton and the associated Q values are not changed. Fig. 14(b) shows that the values of Q_M appear the same in different subranges of initial amplitude A, which indicates that changing A does not change the behaviors of solitons and the solitons exist only within certain subranges of A.

Next, the effects of initial waveform are studied. A Gaussian waveform, frequently used as the fundamental pulse in mode-locked lasers, is chosen. The initial Gaussian waveform is normalized as

$\psi(0,t) = 2\exp[-t^2/(2.547t_0^2)]$, having the same Q value at $z = 0$ with the initial waveform of $2\,\mathrm{sech}(t/t_0)$.

Consider the same parameters, $D = -0.6$ and $-0.004 \le \mu \le -0.001$, as applied to the sech waveform in the previous discussions. It is found that $Q_M = 97.52$ over $1.3 \le A \le 9.7$, $12.4 \le A \le 14.3$

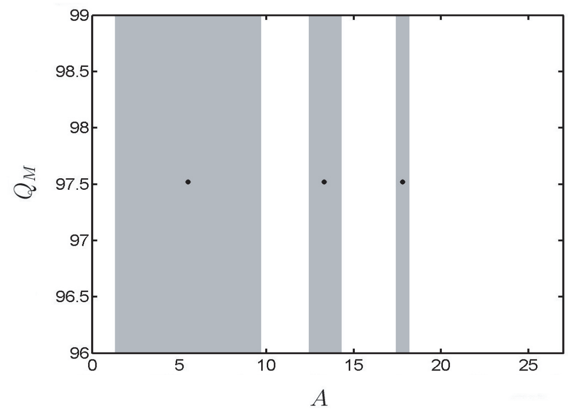

Figure 15. Q_M versus A with $(D, \nu, \delta, \xi, \mu, \tau) = (-0.6, 0.1, -0.1, 0.95, -0.001, 0.125)$, and the initial waveform is $\psi(0,t) = A\exp[-t^2/(2.547t_0^2)]$.

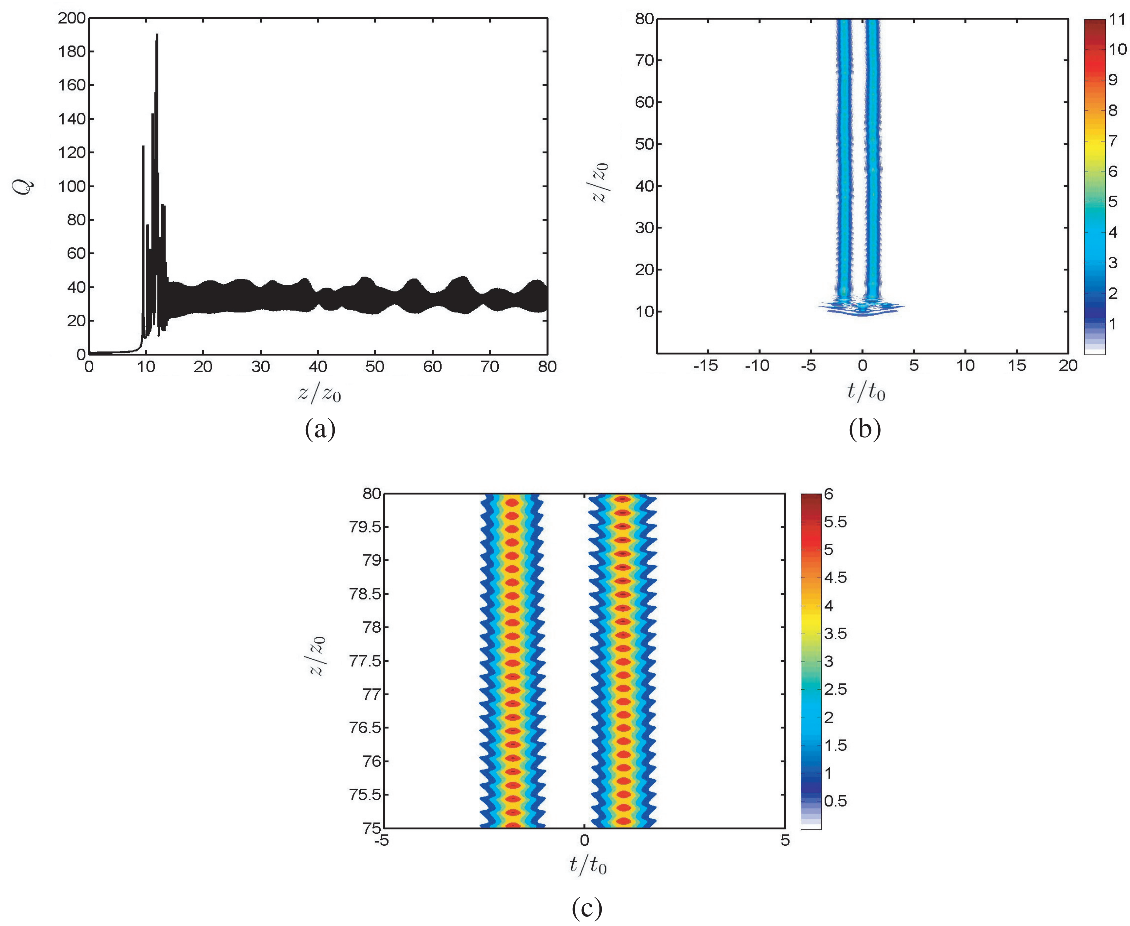

Figure 16. (a) Q versus z with a Gaussian initial waveform, (b) evolution over $z/z_0 \le 80$ and (c) evolution over $75 \le z/z_0 \le 80$; $A = 24.2$, $\mu = -0.003$, other parameters are the same as in Fig. 15.

and $17.4 \leq A \leq 18.2$ at $\mu = -0.001$; $Q_M = 53.51$ over $1.2 \leq A \leq 10.9$, $13.3 \leq A \leq 16.0$, $19.2 \leq A \leq 20.9$ and $25.0 \leq A \leq 26.1$ at $\mu = -0.002$; $Q_M = 23.91$ over $1.2 \leq A \leq 12.1$, $14.3 \leq A \leq 17.9$ and $21.1 \leq A \leq 24.2$ at $\mu = -0.003$. At $\mu = -0.004$, a stationary soliton appears, with $Q = 16.85$ over $1.2 \leq A \leq 13.4$, $15.1 \leq A \leq 20.2$ and $23.3 \leq A \leq 28.1$. Fig. 15 shows the values of Q_M versus A, with $\mu = -0.001$. The soliton type is not affected by the initial amplitude A, and the Q_M values are the same as in the sech waveform, although the valid subranges of A are different from those of the latter.

Consider an interesting case, with $\mu = -0.003$ and $A = 24.2$, the upper bound in the amplitude subrange. As Fig. 12 shows two emerging solitons with constant amplitudes, Figs. 16(a) and 16(b) show two pulsating-like solitons emerging at $z/z_0 > 15$. Fig. 16(c) is an enlarged plot of Fig. 16(b), which shows that two pulsating-like solitons are coupled to each other in the sense that when one grows in amplitude, the other declines. Fig. 16(a) shows that this coupling phenomenon is not perfectly periodical in z.

In summary, there exist valid subranges of initial amplitude over which mode-locking of solitons can be activated. The shape of initial waveform does not affect the soliton type, but it may affect the valid subranges of initial amplitude. The soliton has the same set of Q_M's within the allowable subranges of initial amplitude. Two solitons may emerge if the initial amplitude is near the upper bound of amplitude subranges.

6. CONCLUSION

The split-step Fourier method has been applied to solve the CQGLE for passive mode-locked laser. The soliton solutions can be categorized into stationary, pulsating and chaotic types on a μ-D parametric plane. Based on the soliton waveforms, the boundary between pulsating and chaotic regions can be divided into several distinct zones. The transformation between a stationary soliton and a pulsating one is gradual across the boundary. The effects of initial amplitude and initial waveform on the soliton type have also been studied.

ACKNOWLEDGMENT

This work is partly sponsored by the Ministry of Science and Technology, Taiwan, R. O. C., under contract MOST 105-2221-E-002-035.

REFERENCES

1. Grelu, Ph. and N. Akhmediev, "Dissipative solitons for mode-locked lasers," *Nature Photonics*, Vol. 6, 84–90, 2012.
2. Akhmediev, N., J. M. Soto-Crespo, and G. Town, "Pulsating solitons, chaotic solitons, period doubling, and pulse coexistence in mode-locked lasers: Complex Ginzburg-Landau equation approach," *Phys. Rev. E*, Vol. 63, 056602, 2001.
3. Soto-Crespo, J. M., N. Akhmediev, and A. Ankiewicz, "Pulsating, creeping, and erupting solitons in dissipative systems," *Phys. Rev. Lett.*, Vol. 85, 2937, 2000.
4. Chang, W., J. M. Soto-Crespo, P. Vouzas, and N. Akhmediev, "Extreme amplitude spikes in a laser model described by the complex Ginzburg-Landau equation," *Opt. Lett.*, Vol. 40, No. 13, 2949, 2015.
5. Triki, H., F. Azzouzi, and P. Grelu, "Multipole solitary wave solutions of the higher-order nonlinear Schrödinger equation with quintic non-Kerr terms," *Opt. Commun.*, Vol. 309, 71–79, 2013.
6. Zakeri, G. A. and E. Yomba, "Dissipative solitons in a generalized coupled cubic-quintic Ginzburg-Landau equations," *J. Phys. Soc. Japan*, Vol. 82, 084002, 2013.
7. Saha, M. and A. K. Sarma, "Solitary wave solutions and modulation instability analysis of the nonlinear Schrödinger equation with higher order dispersion and nonlinear terms," *Commun. Nonlinear Sci. Num. Simu.*, Vol. 18, 2420–2425, 2013.

8. Triki, H., F. Azzouzi, and P. Grelu, "An efficient split-step compact finite difference method for cubic-quintic complex Ginzburg-Landau equations," *Computer Phys. Commun.*, Vol. 184, 1511–1521, 2013.
9. Green, P. D., D. Milovic, D. A. Lott, and A. Biswas, "Optical solitons with higher order dispersion by semi-inverse variational principle," *Progress In Electromagnetics Research*, Vol. 102, 337–350, 2010.
10. Runge, A. F. J., N. G. R. Broderick, and M. Erkintalo, "Observation of soliton explosions in a passively mode-locked fiber laser," *Optica*, Vol. 2, 36–39, 2015.
11. Cartes, C. and O. Descalzi, "Periodic exploding dissipative solitons," *Phys. Rev. A*, Vol. 93, 031801, 2016.
12. Chang, W., J. M. Soto-Crespo, P. Vouzas, and N. Akhmediev, "Extreme soliton pulsations in dissipative systems," *Phys. Rev. E*, Vol. 92, 022926, 2015.
13. Soto-Crespo, J. M., M. Grapinet, P. Grelu, and N. Akhmediev, "Bifurcations and multiple-period soliton pulsations in a passively mode-locked fiber laser," *Phys. Rev. E*, Vol. 70, 066612, 2004.
14. Akhmediev, N., J. M. Soto-Crespo, M. Grapinet, and P. Grelu, "Dissipative soliton pulsations with periods beyond the laser cavity round trip time," *J. Nonlinear Optical Phys. Materials*, Vol. 14, No. 2, 177–194, 2005.
15. Tsoy, E. N. and N. Akhmediev, "Bifurcations from stationary to pulsating solitons in the cubic-quintic complex Ginzburg-Landau equation," *Phys. Lett. A*, Vol. 343, 417–422, 2005.
16. Chang, W., A. Ankiewicz, N. Akhmediev, and J. M. Soto-Crespo, "Creeping solitons in dissipative systems and their bifurcations," *Phys. Rev. E*, Vol. 76, 016607, 2007.
17. Weiner, A. M., *Ultrafast Optics*, John Wiley, 2009.
18. Agrawal, G. P., *Nonlinear Fiber Optics*, Academic Press, 2012.
19. Soto-Crespo, J. M., N. Akhmediev, and G. Town, "Continuous-wave versus pulse regime in a passively mode-locked laser with a fast saturable absorber," *J. Opt. Soc. Am. B*, Vol. 1, 234–242, 2002.